Optica Applicata, Vol. LIV, No. 1, 2024
DOI: 10.37190/oa240107

Design of localized surface plasmon resonance-based refractive index sensor using optical fiber

MUKTI YADAV*, R.S. KALER

Thapar Institute of Engineering and Technology, Punjab-147004, India

*Corresponding author: muktiyadav2216@gmail.com

The paper proposes a design of a localized surface plasmon resonance-based refractive index sensor for the detection of a chemical compound availing unclad geometry of the optical fiber. The geometry is explored to analyze the sensing behavior and coupling phenomenon at the metal-dielectric interface. The finite element method (FEM) is applied numerically to evaluate the analytical change in the reflectance spectra of the fiber model by inoculating potassium nitrate compound. The resonance shift and reflectance of the surface plasmon resonance (SPR) signal obtained after the optimization of structural parameters enhance the sensing performance of the prototype. The sensor exhibits a maximum sensitivity of 80.2919 rad/RIU for a 1.56 high refractive index analyte and minimum sensitivity of 2.3446 rad/RIU for a 1.33 low refractive index analyte. The proposed sensor is modelled in such a way that it can be employed in various sensing applications for a wide range of refractive indices.

Keywords: localized surface plasmon resonance (LSPR), multi-mode optical fiber, refractive index sensor, sensitivity, COMSOL Multiphysics.

1. Introduction

Sensing devices are essential in determining various factors related to human lives. They have been employed in various fields like healthcare, agriculture, the chemical industry, biosensing and civil areas for decades [1]. Among them, optical sensors play a more beneficial role than any other device for analyte sensing applications due to their high sensitivity, immunity to electromagnetic interference, small size, and compatibility with remote sensing applications [2]. These sensors lie on the principle of guiding light signals through an optical fiber and detecting changes in the transmitted light due to the presence of the target parameter. The change in the plasmonic characteristics of the optical fiber makes them plasmonic sensors called surface plasmon resonance (SPR) sensors which are the probes that use small amounts of metal nanoparticles on the optical fiber surface [3, 4]. In recent years, the focus has shifted towards localized surface plasmon resonance (LSPR) from conventional SPR which is way more sensitive to changes in the optical properties since they offer improved sensitivity and resolution [5]. LSPR is a phenomenon that occurs when light is coupled with metal

nanoparticles, leading to the excitation of collective oscillations of electrons on the metal surface. This results in the absorption and scattering of light, creating a localized surface plasmon resonant mode [6].

Another vital advantage of LSPR sensors is their ability to detect both refractive index changes and changes in the absorption of the surrounding environment [7]. This is because LSPR sensors can detect changes in the resonant wavelength and the resonance linewidth, which are related to the refractive index and the absorption of the surrounding environment [8]. LSPR-based chemosensors are highly sensitive and selective tools compared to traditional chemosensors that can detect various chemical species in a wide range of applications including environmental monitoring, medical diagnostics, food safety, homeland security *etc*. [9,10]. One of the applications applies to the detection of nitrate compounds. Nitrate is a common pollutant in water, and excessive nitrate levels can cause health problems, particularly for infants and pregnant women. High levels of nitrate in water can also lead to eutrophication. By detecting nitrate levels in real-time people can take action to reduce the levels of nitrate in water and food and prevent contamination [11]. Thus, LSPR-based chemosensors can be used to detect nitrate compounds, offering a highly sensitive and specific method to measure the change in the refractive index [12]. Traditional chemosensors typically work by using a chemical reaction between the target analyte and a sensing material to produce a measurable signal. The sensing material can be a fluorescent dye, electroactive molecule, or other chemical species that undergoes a change in its optical or electrical properties upon interaction with the analyte [13]. On the other hand, LSPR-based chemosensors work by exploiting the LSPR effect when the nanoparticles are in close proximity to each other or to a surface, their LSPR response can be strongly affected by the presence of analyte molecules or the refractive index of the surrounding medium, leading to a change in the nanoparticles' absorbance spectra. They also do not require labelling or complex sample preparation and can be used in complex biological or environmental matrices [14]. However, they can be more expensive and require more specialized equipment than traditional chemosensors.

Most of the refractive index sensors research is confined to low refractive index media ranging from 1.3 to 1.38 [15]. Recent advances in nanofabrication, optical fiber technology, and numerical simulation have greatly improved the performance and capabilities of these sensors. However, some of the parameters still hold a part of the limitation; different materials like aluminium, silver and copper are used for the plasmonic interfaces, but the limiting factor is the formation of an oxide layer onto the surface of the nanoparticles that damps the LSPR response [16]. Modal dispersion can be a major limiting factor for high-speed data transmission and sensing performance in multi-mode optical fibers which can be minimized by selecting appropriate fiber geometries, such as graded-index fibers, LSPR-based fiber sensors, and photonic crystal fibers *etc*. [17].

In this paper, we have contemplated upon the mentioned limitations and aim to design and analyze the optical fiber geometry by optimizing the structural parameters. Due to their unique optical properties, a monolayer of gold nanoparticles (AuNPs) has

been employed to efficiently carry out LSPR phenomenon. Since these nanoparticles exhibit strong light absorption and scattering in visible and near-infrared regions, they are ideal for LSPR sensing applications [18]. Further, the investigation has been done to analyze the sensor response for the detection of potassium nitrate (chemical compound) as the single compound exhibits three morphologies having three different refractive indices: 1.335, a low refractive index and 1.56, a high refractive index, respectively. The numerically simulated results illustrate the efficient performance of the sensor for the high index medium, which has not been done previously to the best of our knowledge. The change in the LSPR response exhibits the efficiency of the proposed refractive index sensor and utilizing this information, makes it possible to design and develop a fiber-based sensing system with improved sensitivity, stability, and robustness, appealing to a wide range of chemo-sensors.

2. Structural design and numerical analysis

Simulation and analysis methods for multimode optical fiber (MMOF) mode with specifications can play an essential role in designing and optimizing multimode fiber (MMF)-based systems. There are various methods that can be used to simulate and analyze the mode properties of MMF, including numerical simulation techniques such as the finite difference method (FDM) and the finite element method (FEM) [19]. These methods can accurately model the propagation of light in MMF, considering the factors such as refractive index profile, bending, and external perturbations [20].

The results are modelled based on the FEM technique. The geometry of the MMF sensor is constructed on a two-dimensional plane using a wave optics module for frequency domain analysis operating at 633 nm wavelength. AuNP layer is coated onto the decladded fiber core with the core and cladding diameters of 20 and 25 μm, respectively. Figure 1 shows the basic fiber geometry considered for the LSPR simulation process. The model encompasses an assumption to draw out the small portion of the middle section of the cladding to expose the fiber core. The monolayer of AuNPs is coated onto the decladded portion to carry out the evanescent wave propa-

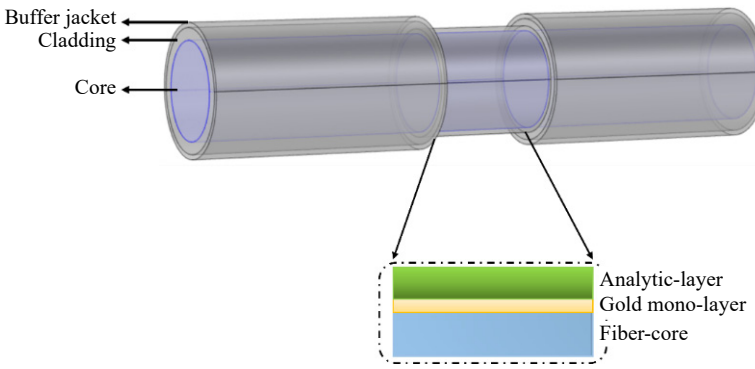

Fig. 1. 3D-fiber geometry in COMSOL.

gation at the metal and dielectric interface. The AuNP layer works as a sensing interface for the analyte layer, whose refractive index can be varied by considering the refractive index model study.

The above 3D geometry is refined into a 2D structure using three consecutive rectangular slabs for the fiber core, gold layer and analyte layer, respectively, as shown in Fig. 1 for further modelling the proposed sensor. The core appraised for modelling comprises SCHOTT n-BK7 material since N-BK7 is a pure universal optical glass made by SCHOTT. It is one of the most common standard glass types used to produce high-quality optics, mainly for the visible spectrum. Its properties consist of a high refractive index homogeneity of 1.509. For the AuNP monolayer coating of thickness 50 nm, we have considered Lorentz and Drude's model [21] with 1.143 relative permittivity and 4.11×10^7 S/m electrical conductivity. Figure 2 illustrates the real part of the gold nanoparticles layer appropriated for the LSPR effect.

Once the geometry of the proposed refractive index (RI) sensor is created, appropriate meshing is applied since FEM is heavily mesh dependent and will compute on infinitely small elements. For relevant meshing, extremely fine mesh is applied all

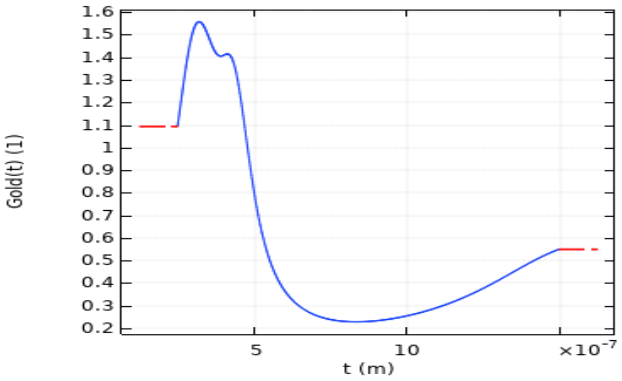

Fig. 2. Refractive index of AuNPs for Lorentz–Drude model.

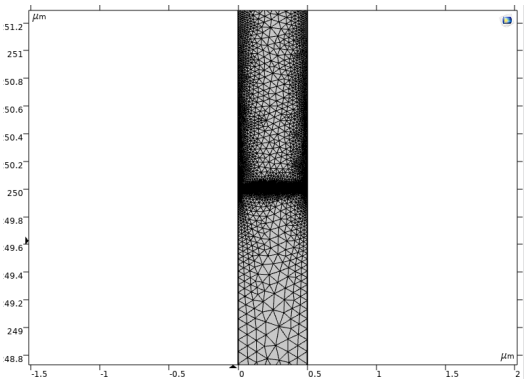

Fig. 3. Meshing of the proposed sensor.

T a b l e 1. Calculated parameters for the sensor simulation.

Parameter	Values	Description
RI_{core}	1.5168	Refractive index of BK7
RI_{medium}	1	Refractive index of air
λ_0	633 nm (6.33×10^{-7} m)	Operating wavelength
$f_0 = c_{const}/\lambda_0$	4.7361×10^{14} 1/s	Operating frequency
p	1500 nm (1.5×10^{-6} m)	Period of dielectric
t_d	50 nm (5×10^{-8} m)	Thickness of AuNP layer
α	0 rad	Angle of incidence, parameter
ε_r	–11.6	Real permittivity of Au at 633 nm
ε_i	1.2	Imaginary permittivity of Au at 633 nm

throughout the geometry as shown in Fig. 3. The parameters, as shown in Table 1, are applied to estimate the input values for a created model. The parameters inured enable us to evaluate the computational results for the surface plasmon phenomenon on the modelled geometry.

The analysis of periodic arrays of AuNPs was performed by setting the boundary condition at the sidewalls of the rectangular slab. The height of the dielectric material can be chosen from the following equation [22]:

$$H \approx 10\frac{1}{\sqrt{K_o^2 - K_{spp}^2}}$$

where,

$$K_{spp} = K_o\sqrt{\frac{\varepsilon_m\varepsilon_d}{\varepsilon_m + \varepsilon_d}}$$

and ε_m is the permittivity of the metal, ε_d is the relative permittivity of the dielectric. To analyze the single nanoparticle and periodic arrays investigation, the perfect electric conductor (PEC) condition and the periodic boundary condition are applied to the study. In and Out ports of model were defined for top and bottom surfaces, respectively, to define the linearly polarized incident waves and to calculate reflection coefficients [23].

3. Results and discussions

The proposed sensor is based on wave excitation at the metal-dielectric interface giving rise to the evanescent wave absorption phenomenon and promoting a shift in the LSPR reflectance dip. One crucial aspect in designing and optimizing MMF-based sensors is the determination of the mode analysis, which describes the temporal spreading of light pulses as they propagate through the fiber. Figure 4 (a) represents the built geometry, and (b) represents the respective SPR modes propagating in the *z*-direction at the metal and dielectric interface at which the electric field gets distributed around the

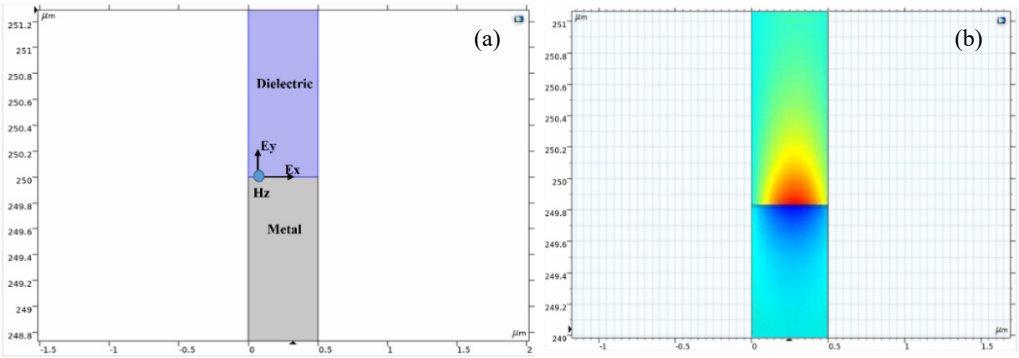

Fig. 4. (a) 2D model of metal and dielectric interface and (b) SPP modes propagating at metal-dielectric interface.

layer of AuNP. The phenomenon results from the coupling between the fiber-guided modes (fundamental modes) and the SPP (surface plasmon polaritons) modes at resonant conditions [5]. The modal dispersion can be measured experimentally by injecting light pulses into the fiber and observing their temporal profile at the output or by numerical simulation methods, such as the FDM.

When light illuminates the metal-dielectric interface, the electromagnetic field generated by SPR enhances the light absorption and induces a characteristic dip in the reflection spectrum. This dip, also known as the SPR dip or SPR angle, provides a sensitive measure of changes in the refractive index near the metal-dielectric interface, which can be used to detect and quantify various analytes, including biomolecules and chemicals. Three refractive indices (RIs) of the same chemical compound potassium nitrate have been used to investigate the performance of the proposed refractive index sensor. Potassium nitrate (KNO_3) is a crystalline salt having three chemical frameworks with the index of refraction: 1.335 (alpha), 1.5056 (beta), 1.5604 (gamma) [22]. Furthermore, making use of the RIs of the KNO_3 compound we have observed a spectral shift in the reflectance graph.

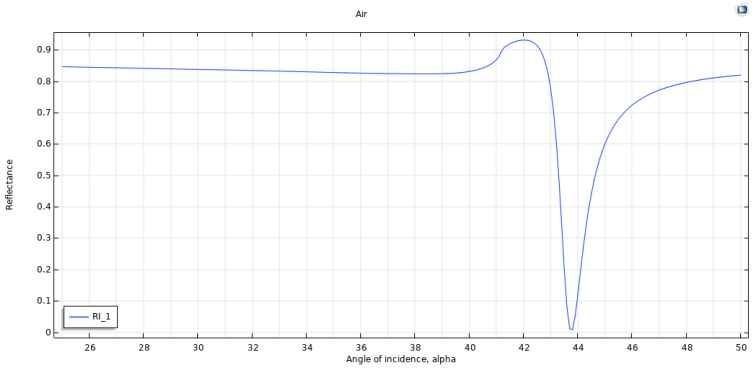

Fig. 5. Reflectance spectra of air.

Initially, the investigation is carried out for air media which serves as a reference for other refractive indices changes. The geometry includes the layer of fiber-glass, AuNP layer and air with a refractive index of 1. Figure 5 illustrates the reflectance spectra of air with a dip at 43.8 angle of incidence and 0.00753 (approximately 0) reflectance unit. The graph depicts that when air is taken as a refractive medium, the reflected light grazes over the surface of the fiber core and hence gets fully transmitted at the output end.

Now we consider the three different RIs of the KNO_3 compound alpha, beta and gamma, respectively. Figure 6 demonstrates the variation in the reflectance curve of alpha, beta and gamma refractive indices along the *x*-axis with a considerable shift in the angle of incidence at 34.8, 35.2 and 39.6, respectively, and changes in the intensity of the reflectance unit are 0.76549, 0.73359 and 0.6101, respectively. The graph depicts that while increasing the refractive index of the medium there is an increase in the corresponding incident angle as shown in inset graph. The *x*-axis corresponds to the different refractive indices with refractive index unit (RIU) displaying a linear response curve.

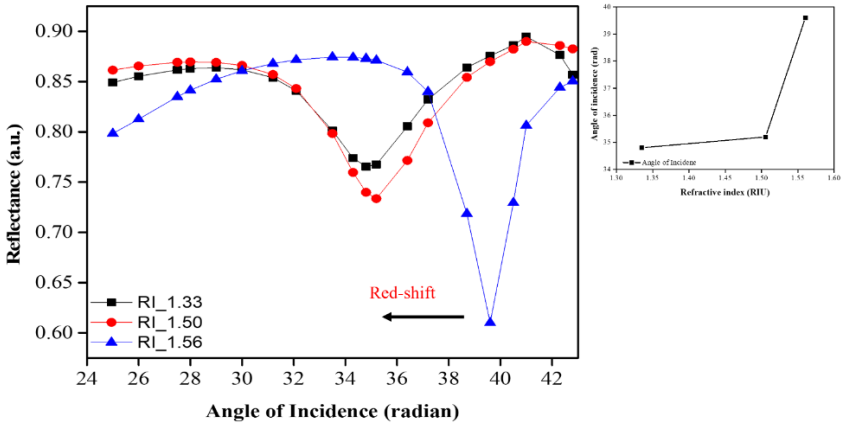

Fig. 6. Reflectance plot for alpha, beta and gamma RIs of KNO_3.

Figure 7 illustrates the red-shifts in the angle of incidence and reflectance unit of all three RIs alpha, beta and gamma with respect to air. The air acts as a reference for the other medium and any change due to analyte RI (n_a) will affect the response of the sensor as well as the sensitivity of the design. It is also noticed that there is a considerable shift in the reflectance unit of the three RIs. Table 2 summarizes the LSPR and reflectance shift among the different RIs with respect to the air.

Any small shift in the reflectance spectra dip indicates the analyte RI change. The obtained reflectance curve shows that if the refractive index of the analyte is increased, then the dip of the curve shifts towards the longer incident angle but the shift with respect to air reference is a red shift towards shorter angle of incidence. Table 2

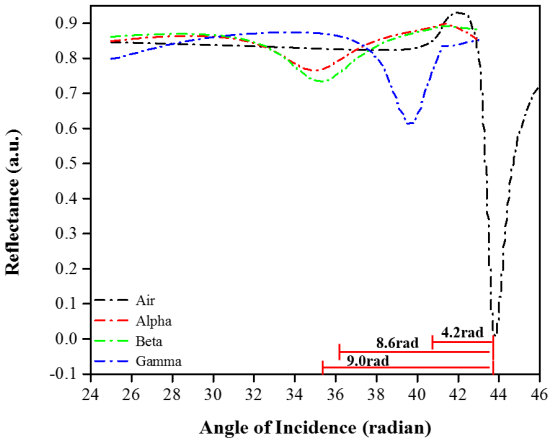

Fig. 7. Red shift in the LSPR of the KNO_3 RIs with respect to air.

T a b l e 2. Obtained parameters for the three RIs and their corresponding shifts.

Refractive indices of KNO_3	Angle of incidence (*x*-axis; radians)	Reflectance (*y*-axis; a.u.)	Change in LSPR spectra with respect to air [rad]
Alpha – 1.335	34.8	0.76549	9.0
Beta – 1.5056	35.2	0.73359	8.6
Gamma – 1.5604	39.6	0.6101	4.2

shows the summarized parameters for the spectral changes and shift in reflectance intensity.

According to Snell's law, the refractive index is directly proportional to the sine of the angle of incidence and is inversely proportional to the reflection of light. Thus, from Table 2, we can infer that while increasing the refractive index of the surrounding medium of the AuNPs, the angle of incidence is increasing. Thus, Fig. 8 represents the

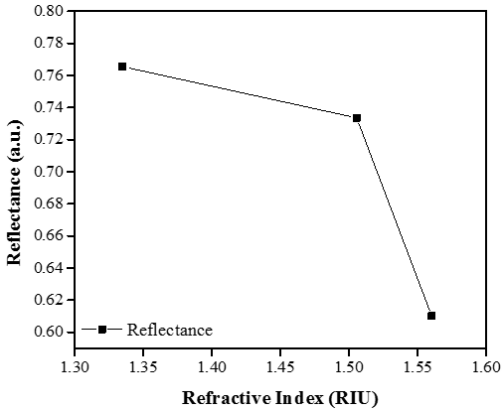

Fig. 8. Refractive index *versus* reflectance curve.

graph of RI *versus* reflectance which states that while increasing the refractive index of the surrounding medium, the reflection intensity of the light decreases. In other words, when we increase the refractive index most of the evanescent light gets absorbed into the denser medium which results in less propagation of the reflected light at the output.

Sensitivity is an important parameter that defines the sensor's performance and efficiency and should be optimized to higher levels. A change in RI of the medium causes change in the reflectance properties of the fiber which affects the LSPR-based sensor's sensitivity [24]. The sensitivity (S_n) equation in terms of variation of RI with respect to wavelength is given by [25]:

$$S_n = \frac{\Delta\lambda}{\Delta n} \quad \left[\frac{\text{nm}}{\text{RIU}}\right]$$

where, $\Delta\lambda$ is the spectral shift in the wavelength and Δn is the change in refractive index.

There are two types of sensitivity: one is amplitude sensitivity S_A given by the change in the intensity of the reflected light ΔR to the change in refractive index Δn. The values calculated for S_A (RIU^{-1}) of refractive indices 1.335, 1.5056 and 1.5604 are 2.262, 1.4360 and 1.07524, respectively.

The second one is wavelength sensitivity S_W which is calculated by a change in wavelength or shift in wavelength to the change in refractive index. In our simulated result, the wavelength sensitivity is defined in terms of change in angle of incidence $\Delta\alpha$ to the change in refractive index Δn denoted by S_W (rad/RIU). The calculated values of S_W for the mentioned RIs are 26.865, 17.009 and 7.494, respectively.

Table 3 shows the calculated sensitivity values of the reported RIs of potassium nitrate with respect to change in air values.

T a b l e 3. Sensitivity of the proposed refractive index sensor.

Δn	$\Delta\alpha$ [rad]	ΔR [a.u.]	S_W [rad/RIU]	S_A [RIU^{-1}]
1.335–1.5056	9	0.75796	2.3446	4.442907
1.335–1.5604	8.6	0.72606	21.29547	3.2212067
1.5056–1.5604	4.2	0.60257	80.29197	2.2534671

T a b l e 4. Comparison of other RI sensors with the proposed sensor in terms of sensitivity.

Sensor design	Binding molecule	RI range	Sensitivity
LSPR-based optical fiber sensor [17]	Silver nanowires	1.27–1.33	3725 nm/RIU
LSPR-based photonic crystal fiber [24]	Gold and aluminium doped zinc oxide	1.27–1.45	46300 nm/RIU
LSPR-based concave shaped optical fiber sensor [25]	Gold nanowires	1.33–1.38	4471 nm/RIU
LSPR-based optical fibre sensor (proposed)	Gold film	1.33–1.56	80.29197 rad/RIU

Table 4 shows the comparison of various other LSPR-based refractive index sensors with the presented RI sensor in terms of their sensitivity. Thus, we can infer from the above results that optical fiber sensors are efficient to be used as refractive index sensors for high as well as low refractive index values of the analyte. The results show that LSPR-based sensors have high sensitivity of 80.29197 rad/RIU for higher refractive index and 4.443 RIU^{-1} sensitivity for low refractive index media difference in terms of amplitude, making them a promising platform for chemo-sensing applications. The paper demonstrates the potential of optimizing the sensitivity of the LSPR-based multimode optical fiber sensors in the detection of the change in refractive index induced by chemical compounds and structures.

4. Conclusion

The research highlights the design of a refractive index sensor based on LSPR phenomenon with sensitivity in terms of incident angle for low and high refractive index values. The sensor performance was analyzed and simulated by the finite element method using the COMSOL Multiphysics tool. The results show that the sensor has high sensitivity of 80.29197 rad/RIU for higher refractive index of 1.5604 and 4.443 RIU^{-1} sensitivity for low refractive index media of 1.335 in terms of difference in amplitude. The design and analysis of LSPR-based MMOF sensor using numerical simulations has proven to be a powerful and effective tool in optimizing the parameters such as geometry, metal coating thickness, and refractive index which can lead to improved sensitivity, selectivity, and resolution. Despite many benefits, the design and implementation of these sensors are still in the early stages of development.

As this field continues to grow, we can expect the development of even more sensitive and robust LSPR-based sensors for a broader range of applications. Numerical simulations and geometry design hold a promising future for the advancement of sensor technology and its applications in other aspects.

References

[1] CHAUHAN M., SINGH V.K., *Review on recent experimental SPR/LSPR based fiber optic analyte sensors*, Optical Fiber Technology **64**, 2021: 102580. https://doi.org/10.1016/j.yofte.2021.102580

[2] SABRI N., ALJUNID S.A., SALIM M.S., AHMAD R.B., KAMARUDDIN R., *Toward optical sensors: Review and applications*, Journal of Physics: Conference Series **423**(1), 2013: 012064. https://doi.org/10.1088/1742-6596/423/1/012064

[3] SEPÚLVEDA B., ANGELOMÉ P.C., LECHUGA L.M., LIZ-MARZÁN L.M., *LSPR-based nanobiosensors*, Nano Today **4**(3), 2009: 244-251. https://doi.org/10.1016/j.nantod.2009.04.001

[4] GUPTA B.D., VERMA R.K., *Surface plasmon resonance-based fiber optic sensors: Principle, probe designs, and some applications*, Journal of Sensors, Vol. 2009, 2009: 979761. https://doi.org/10.1155/2009/979761

[5] DORMENY A.A., SOHI P.A., KAHRIZI M., *Design and simulation of a refractive index sensor based on SPR and LSPR using gold nanostructures*, Results in Physics **16**, 2020: 102869. https://doi.org/10.1016/j.rinp.2019.102869

[6] Caucheteur C., Guo T., Albert J., *Review of plasmonic fiber optic biochemical sensors: Improving the limit of detection*, Analytical and Bioanalytical Chemistry **407**, 2015: 3883-3897. https://doi.org/10.1007/s00216-014-8411-6

[7] Hammond J.L., Bhalla N., Rafiee S.D., Estrela P., *Localized surface plasmon resonance as a biosensing platform for developing countries*, Biosensors **4**(2), 2014: 172-188. https://doi.org/10.3390/bios4020172

[8] Lodewijks K., Van Roy W., Borghs G., Lagae L., Van Dorpe P., *Boosting the figure-of-merit of LSPR-based refractive index sensing by phase-sensitive measurements*, Nano Letters **12**(3), 2012: 1655-1659. https://doi.org/10.1021/nl300044a

[9] Cusano A., Pilla P., Contessa L., Iadicicco A., Campopiano S., Cutolo A., Giordano M., Guerra G., *High-sensitivity optical chemosensor based on coated long-period gratings for sub-ppm chemical detection in water*, Applied Physics Letters **87**(23), 2005: 234105. https://doi.org/10.1063/1.2136437

[10] Kräмer J., Kang R., Grimm L.M., De Cola L., Picchetti P., Biedermann F., *Molecular probes, chemosensors, and nanosensors for optical detection of biorelevant molecules and ions in aqueous media and biofluids*, Chemical Reviews **122**(3), 2022: 3459-3636. https://doi.org/10.1021/acs.chemrev.1c00746

[11] Alahi M.E.E., Mukhopadhyay S.C., *Detection methods of nitrate in water: a review*, Sensors and Actuators A: Physical **280**, 2018: 210-221. https://doi.org/10.1016/j.sna.2018.07.026

[12] Sepahvand M., Ghasemi F., Hosseini H.M., *Accelerated leaching of unmodified gold nanoparticles for environmental and biological monitoring of nitrite and nitrate*, ChemistrySelect **7**(3), 2022: e202103094. https://doi.org/10.1002/slct.202103094

[13] Prodi L., *Luminescent chemosensors: From molecules to nanoparticles*, New Journal of Chemistry **29**(1), 2005: 20-31. https://doi.org/10.1039/B411758A

[14] Barbillon G., Bijeon J.-L., Plain J., de la Chapelle M.L., Adam P.-M., Royer P., *Electron beam lithography designed chemical nanosensors based on localized surface plasmon resonance*, Surface Science **601**(21), 2007: 5057-5061. https://doi.org/10.1016/j.susc.2007.09.005

[15] Pathak A.K., Rahman B.M.A., Singh V.K., Kumari S., *Sensitivity enhancement of a concave shaped optical fiber refractive index sensor covered with multiple Au nanowires*, Sensors **19**(19), 2019: 4210. https://doi.org/10.3390/s19194210

[16] Szunerits S., Boukherroub R., *Sensing using localised surface plasmon resonance sensors*, Chemical Communications **48**(72), 2012: 8999-9010. https://doi.org/10.1039/C2CC33266C

[17] Cao J., Sun T., Grattan K.T.V., *Gold nanorod-based localized surface plasmon resonance biosensors: A review*, Sensors and Actuators B: Chemical **195**, 2014: 332-351. https://doi.org/10.1016/j.snb.2014.01.056

[18] Singh P.K., Singh V.K., Chualya S.K., *Numerical analysis of LSPR based fiber sensor for low refractive index detection*, Optik **224**, 2020: 165704. https://doi.org/10.1016/j.ijleo.2020.165704

[19] Sharma A.K., Pandey A.K., Kaur B., *A review of advancements (2007–2017) in plasmonics-based optical fiber sensors*, Optical Fiber Technology **43**, 2018: 20-34. https://doi.org/10.1016/j.yofte.2018.03.008

[20] Centeno A., *Improved Drude-Lorentz dielectric function for gold nanospheres*, arXiv:2012.05090 [physics.optics]. https://doi.org/10.48550/arXiv.2012.05090

[21] Al-Janaby N., Al-Dergazly A., *Fabrication of multi-mode tip fiber sensor based on surface plasmon resonance (SPR)*, Sustainable Engineering and Innovation **2**(1), 2020: 10-17. https://doi.org/10.37868/sei.v2i1.27

[22] Colombelli A., Manera M.G., Rella R., Vasanelli L., *FEM modeling of nanostructures for sensor application*, [In] Di Natale C., Ferrari V., Ponzoni A., Sberveglieri G., Ferrari M. [Eds.] *Sensors and Microsystems. Lecture Notes in Electrical Engineering*, Vol. 268, Springer, Cham. https://doi.org/10.1007/978-3-319-00684-0_55

[23] Elvers B., *Ullmann's Encyclopedia of Industrial Chemistry*, Vol. 17, Hoboken, NJ, Verlag Chemie, 1991.

[24] TARIQ S.M., FAKHRI M.A., SALIM E.T., HASHIM U., ALSULTANY F.H., *Design of an unclad single-mode fiber-optic biosensor based on localized surface plasmon resonance by using COMSOL Multiphysics 5.1 finite element method*, Applied Optics **61**(21), 2022: 6257-6267. https://doi.org/10.1364/AO.458175

[25] RAKIBUL ISLAM M., IFTEKHER A.N.M., ANZUM M.S., RAHMAN M., SIRAZ S., *LSPR based double peak double plasmonic layered bent core PCF-SPR sensor for ultra-broadband dual peak sensing*, IEEE Sensors Journal **22**(6), 2022: 5628-5635. https://doi.org/10.1109/JSEN.2022.3149715

Received July 10, 2023